

Article

Modeling and Control of Negative-Buoyancy Tri-Tilt-Rotor Autonomous Underwater Vehicles Based on Immersion and Invariance Methodology

Tao Wang, Chao Wu *, Jianqin Wang and Tong Ge

State Key Laboratory of Ocean Engineering, Collaborative Innovation Center for Advanced Ship and Deep-Sea Exploration, Shanghai Jiao Tong University, Shanghai 200240, China; wangtaonice@sjtu.edu.cn (T.W.); wjq-394805990@163.com (J.W.); tongge@sjtu.edu.cn (T.G.)

* Correspondence: wuchaorr@sjtu.edu.cn; Tel.: +86-021-3420-8063

Received: 16 June 2018; Accepted: 13 July 2018; Published: 15 July 2018

Abstract: Spot hover and high speed capabilities of underwater vehicles are essential for ocean exploring, however, few vehicles have these two features. Moreover, the motion of underwater vehicles is prone to be affected by the unknown hydrodynamics. This paper presents a novel negative-buoyancy autonomous underwater vehicle equipped with tri-tilt-rotor to obtain these two features. A detailed mathematical model is derived, which is then decoupled to altitude and attitude subsystems. For controlling the underwater vehicle, an attitude error model is designed for the attitude subsystem, and an adaptive nonlinear controller is proposed for the attitude error model based on immersion and invariance methodology. To demonstrate the effectiveness of the proposed controller, a three degrees of freedom (DOF) testbed is developed, and the performance of the controller is validated through a real-time experiment.

Keywords: negative-buoyancy; tri-tilt-rotor; autonomous underwater vehicle (AUV); immersion and invariance

1. Introduction

With the increasing demand for marine equipment over the past decades, different types of marine vehicles have been developed to expand human exploration capabilities [1] from the surface to the bottom of the ocean. Underwater vehicles perform various missions, such as collecting samples [2], acquiring data [3], and repairing marine structures [4].

In accordance with the level of autonomy for self-driving vehicles, underwater vehicles can be classified into remotely operated underwater vehicles (ROV) [5], autonomous underwater vehicles (AUV) [6,7], and human occupied vehicles (HOV) [8]. ROV consist of a cable that is used for power supply and as a communication line, which is used by the operator to remotely control the ROV [2,9]; an AUV is autonomous, and it performs motion control and mission planning [10–12]; an HOV has a life support system, and a pilot inside the vehicle controls the movement of the HOV for precise movement. ROV and AUV are unmanned underwater vehicles, and therefore, they have the advantages of no risk to life and long operation time. However, the densities of these vehicles are similar to that of the water owing to the buoyancy of the material used [13,14]. This increases the size and drag force, which considerably slows down the speed of the vehicle [15]. In some scenarios, a high-speed underwater vehicle is required to perform time-sensitive missions. Moreover, with the development of deep sea mining [16], a spot hover is a necessary capability for missions such as recharging and payload transition.

Traditional underwater vehicles have a cylindrical shape or an open frame. Cylindrical-shaped underwater vehicles have the advantage of a low drag force. They are propelled using fixed thrusters,

and some of these vehicles are equipped with vertical and horizon thrusters to provide extra control forces. An ocean glider is an autonomous underwater vehicle used for ocean science [15,17]; it uses a small change of buoyancy in order to ascend and descend. A fixed wing converts the vertical motion to horizontal motion [18], thus acting like a saw tooth pattern [19]. The energy effect is so high that the glider can continually glide over hundreds of kilometers for months. Open frame vehicles such as an ROV can operate at one spot with the help of multiple rotors [20]; the AUV cannot achieve this [21]. However, the cable connecting the ROV to the mother ship limits the work range of the ROV [2]. A kind of negative buoyancy vehicle is designed to achieve high speed and long cruise range, it is more efficient than traditional AUV at high speed. However, it has to fly in the water to maintain depth, besides, spot hover capability is not achieved [22].

The design and control of an underwater vehicle involves many problems such as the nonlinearity of the model [13,21,23], underactuation [24], and the influence of the ocean current, waves, and turbulence [25].

In this paper, we present a negative-buoyancy tri-tilt-rotor autonomous underwater vehicle (NTAUV) to achieve the capability of spot hover and high-speed motion. The NTAUV is illustrated in Figure 1. The NTAUV is heavier than water, has negative buoyancy, and it balances the weight by buoyancy and lift force generated by the fixed wing or thrusters. Further, it operates under three modes: hover, horizontal motion, and transition between them. The NTAUV can hover or slowly cruise by controlling the rotor speed and the tail rotor angle in the hover mode. The hover motion control of NTAUV uses a hierarchical control scheme. The outer layer is position control, and the inner layer is attitude control. Attitude control is the fundamental function of the underactuated system. This paper focuses on hover mode modeling and control, especially attitude control. We design an adaptive nonlinear attitude controller using the immersion and invariance (I&I) methodology.

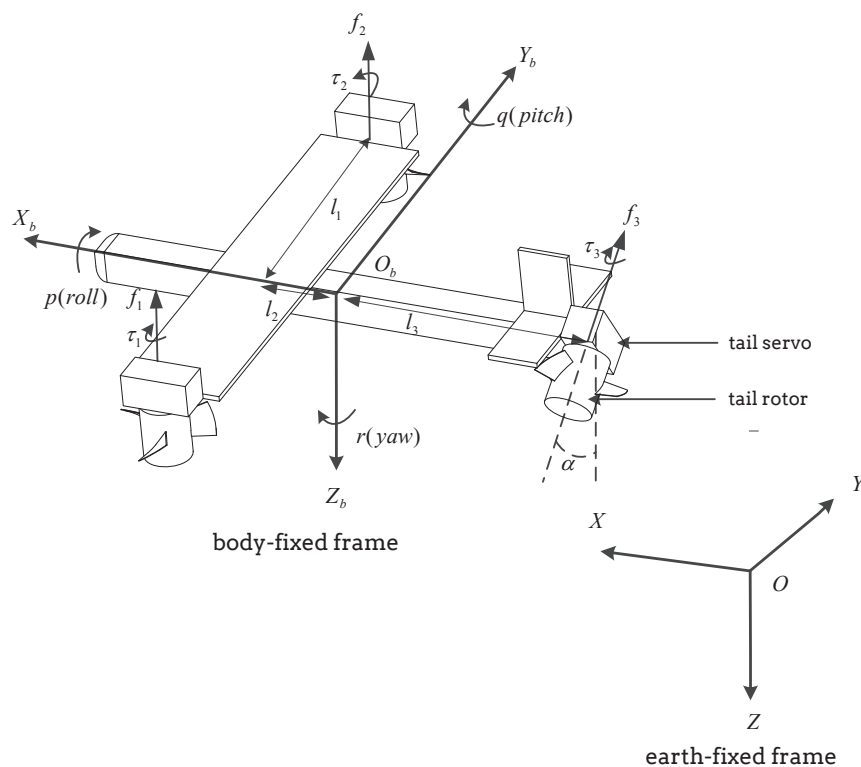


Figure 1. Configuration of NTAUV with Earth-fixed and body-fixed frame.

The article is structured as follows. Section 2 introduces some preliminaries, including the kinematic equations, mechanical structure, mathematical model, and subsystems of altitude and attitude. Section 3.1 presents the attitude error model. In Section 3.2, an adaptive nonlinear I&I

controller is designed for the attitude subsystem. The stability analysis is presented in Section 3.3. A three degree of freedom testbed is designed and the experiment results are shown in Section 4.

2. Preliminaries

2.1. Kinematics and Kinetics

Modeling a marine vehicle involves the study of statics and dynamics. The 6 DOF motion of a marine vehicle is analyzed by defining two coordinate frames, as illustrated in Figure 1. $O_b X_b Y_b Z_b$ is fixed to the vehicle and is called the body-fixed frame. $OXYZ$ is fixed to the earth and is called the earth-fixed frame. The origin of the body-fixed frame is the center of gravity (CG). The center of buoyancy locates at CG.

The notations of the frames used in this paper are [1]

$$\eta = [\eta_1^\top, \eta_2^\top]^\top; \eta_1 = [x, y, z]^\top; \eta_2 = [\phi, \theta, \psi]^\top \tag{1}$$

$$v = [v_1^\top, v_2^\top]^\top; v_1 = [u, v, w]^\top; v_2 = [p, q, r]^\top \tag{2}$$

here η denotes the position and orientation of the vehicle and v denotes the linear and angular velocity of the vehicle.

The rigid body kinematics of the vehicle are given by [1]

$$\dot{\eta}_1 = J_1(\eta_2)v_1 \tag{3}$$

$$\dot{\eta}_2 = J_2(\eta_2)v_2 \tag{4}$$

in which

$$J_1(\eta_2) = \begin{bmatrix} c\psi\theta & -s\psi c\phi + c\psi s\theta s\phi & s\psi s\phi + c\psi c\phi s\theta \\ s\psi c\theta & c\psi c\phi + s\psi s\theta s\phi & -c\psi s\phi + s\psi s\theta c\phi \\ -s\theta & c\theta s\phi & c\theta c\phi \end{bmatrix} \tag{5}$$

$$J_2(\eta_2) = \begin{bmatrix} 1 & s\phi t\theta & c\phi t\theta \\ 0 & c\phi & -s\phi \\ 0 & s\phi/c\theta & c\phi/c\theta \end{bmatrix} \tag{6}$$

where $s \cdot = \sin(\cdot), c \cdot = \cos(\cdot), t \cdot = \tan(\cdot)$.

The mathematical model of the 6 DOF rigid body dynamics is

$$M_{RB}\dot{v} + C_{RB}(v)v = \tau_{RB} \tag{7}$$

where

$$\tau_{RB} = \tau_H + \tau_P \tag{8}$$

τ_H denotes the hydrodynamic forces and moments, and τ_P denotes the propulsion forces and moments. τ_H can be calculated as

$$\tau_H = -M_A\dot{v} - C_A(v)v - D(v)v \tag{9}$$

For underwater vehicles, if the movement is at low speed, it can be assumed that the vehicle performs a non-coupled motion. For simplicity, M_A and $D(v)$ have a diagonal structure with only linear damping terms on the diagonal

$$M_A = -diag\{X_{\dot{u}}, Y_{\dot{v}}, Z_{\dot{w}}, K_{\dot{p}}, M_{\dot{q}}, N_{\dot{r}}\} \tag{10}$$

The Coriolis terms of added mass are

$$C_A(v) = \begin{bmatrix} 0 & 0 & 0 & 0 & -Z_{\dot{w}w} & Y_{\dot{v}v} \\ 0 & 0 & 0 & Z_{\dot{w}w} & 0 & -X_{\dot{u}u} \\ 0 & 0 & 0 & Y_{\dot{v}v} & X_{\dot{u}u} & 0 \\ 0 & -Z_{\dot{w}w} & Y_{\dot{v}v} & 0 & -N_{\dot{r}r} & M_{\dot{q}q} \\ Z_{\dot{w}w} & 0 & -X_{\dot{u}u} & N_{\dot{r}r} & 0 & -K_{\dot{p}p} \\ Y_{\dot{v}v} & X_{\dot{u}u} & 0 & -M_{\dot{q}q} & K_{\dot{p}p} & 0 \end{bmatrix} \quad (11)$$

The damping terms are

$$D(v) = -diag\{X_u, Y_v, Z_w, K_p, M_q, N_r\} \quad (12)$$

For the rigid body, the inertia matrix M_{RB} is

$$M_{RB} = \begin{bmatrix} mI_{3 \times 3} & 0 \\ 0 & I_0 \end{bmatrix} \quad (13)$$

where

$$I_0 = \begin{bmatrix} I_x & -I_{xy} & -I_{xz} \\ -I_{yx} & I_y & -I_{yz} \\ -I_{zx} & -I_{zy} & I_z \end{bmatrix} \quad (14)$$

The Coriolis and centripetal terms are

$$C_{RB}(v) = \begin{bmatrix} 0_{3 \times 3} & -mS(v_1) \\ -mS(v_1) & -S(I_0v_2) \end{bmatrix} \quad (15)$$

Remark 1. The skew-symmetric matrix $S(\lambda)$ is defined as

$$S(\lambda) = \begin{bmatrix} 0 & -\lambda_3 & \lambda_2 \\ \lambda_3 & 0 & -\lambda_1 \\ -\lambda_2 & \lambda_1 & 0 \end{bmatrix} \quad (16)$$

where $\lambda = [\lambda_1, \lambda_2, \lambda_3]^T$. S satisfies $x^T S(v_2)x \equiv 0, x, v_2 \in \mathbb{R}^3$.

Based on the mechanical structure of the vehicle, the propulsion forces f and moments τ acting on the vehicle are [26–28]

$$f = \begin{bmatrix} 0 \\ f_3 \sin \alpha \\ -f_1 - f_2 - f_3 \cos \alpha \end{bmatrix} \quad (17)$$

$$\tau = \begin{bmatrix} l_1(f_1 - f_2) \\ l_2(f_1 + f_2) - l_3 f_3 \cos \alpha - \tau_3 \sin \alpha \\ -l_3 f_3 \sin \alpha + \tau_1 - \tau_2 + \tau_3 \cos \alpha \end{bmatrix} \quad (18)$$

where the force and torque generated by each rotor is

$$\tau_i = k_\tau \omega^2 \quad (19)$$

$$f_i = k_f \omega^2 \quad (20)$$

The total moments (18) can be considered as the sum of the following two terms

$$\tau_m = \begin{bmatrix} l_1(f_1 - f_2) \\ l_2(f_1 + f_2) - l_3 f_3 \cos\alpha \\ -l_3 f_3 \sin\alpha \end{bmatrix} \tag{21}$$

$$\tau_{tail} = \begin{bmatrix} 0 \\ -\tau_3 \sin\alpha \\ \tau_1 - \tau_2 + \tau_3 \cos\alpha \end{bmatrix} \tag{22}$$

Rotor 1 and rotor 2 rotate in the opposite directions; therefore, the moments of the rotors are counteracted. Moreover, $k_\tau \ll k_f$, and τ_{tail} is much smaller compared to the control force, and it can be neglected [26]. Thus, the control force and moment are

$$\tau_P = \begin{bmatrix} f \\ \tau_m \end{bmatrix} \tag{23}$$

Note $M = M_{RB} + M_A, C(v) = C_{RB}(v) + C_A(v)$. Therefore, the whole system can be written as

$$M\dot{v} + C(v)v + D(v) = \tau_P \tag{24}$$

The system (24) has four inputs and six outputs; therefore, it is an underactuated system. We can see that the challenge is the lateral force $f_3 \sin\alpha$ of f in (17). Consider f as

$$f = [0, 0, f_z]^T + \Phi \tau_m \tag{25}$$

where

$$\Phi = \begin{bmatrix} 0 & 0 & 0 \\ 0 & 0 & -1/l_3 \\ 0 & 0 & 0 \end{bmatrix} \tag{26}$$

and

$$f_z = -f_1 - f_2 - f_3 \cos\alpha \tag{27}$$

Note that (21) and (27) define a diffeomorphism, and therefore, the control inputs $[f_1, f_2, f_3, \alpha]^T$ can be recovered from $[f_z, \tau_m^T]^T$ [27].

2.2. Altitude and Attitude Subsystems

The lateral component $f_3 \sin\alpha$ of (17) is the main contributor of the yaw control input; therefore, the 6 DOF system can be decoupled to an altitude subsystem and an attitude subsystem. f_z is the altitude control input and τ_m is the attitude control input.

The altitude equation is

$$(m + Z_{\dot{w}})\ddot{z} - Z_w \dot{z} - (W - B) = f_z \cos\phi \cos\theta \tag{28}$$

where $W = mg$ is the rigid body weight in the air, $B = \rho g \nabla$ is the buoyancy in the water, g is the gravity constant, and ∇ is the displacement.

The attitude equation is

$$(I_0 + I_A)v_2 + (-S((I_0 + I_A)v_2))v_2 + Dv_2 = \tau_m \tag{29}$$

where

$$I_A = -diag\{K_{\dot{p}}, M_{\dot{q}}, N_{\dot{r}}\} \tag{30}$$

$$D = -diag\{K_p, M_q, N_r\} \tag{31}$$

As $S((I_0 + I_A)v_2)v_2 = S(v_2)(I_0 + I_A)v_2$, we rewrite the attitude equation

$$(I_0 + I_A)v_2 - S(v_2)(I_0 + I_A)v_2 + Dv_2 = \tau_m \tag{32}$$

The whole underactuated system is decoupled into two fully actuated subsystems: altitude subsystem and attitude subsystem. We could design the controller separately to control the whole system. The attitude control is the core function of NTAUV; we design the attitude controller in Section 3.

3. Attitude Controller Design

For the NTAUV, which is heavier than water, the attitude control is the essential function for maneuvering control. In general, an attitude controller is designed as the inner loop of a higher level controller, such as path following or trajectory tracking.

In this section, an adaptive I&I attitude controller is designed. I&I is a nonlinear controller design method, and it yields a stabilizing scheme that counters the effect of the uncertain parameters adopting a robustness perspective [29–31]. The stability of the controller is proved in Section 3.3.

3.1. Attitude Error Model

Without loss of generality, the reference attitude is $\eta_{2d} = \eta_{2d}(t)$, therefore, the tracking error is

$$\tilde{\eta}_2 = \eta_2 - \eta_{2d}, \tilde{v}_2 = v_2 - J_2^{-1}(\eta_2)\dot{\eta}_{2d} \tag{33}$$

We define the energy function, which is the sum of the potential and kinetic energy, as

$$H(\tilde{\eta}_2, \tilde{v}_2) = \frac{1}{2}\tilde{\eta}_2^\top K_1 \tilde{\eta}_2 + \frac{1}{2}\tilde{v}_2^\top I^2 \tilde{v}_2 \tag{34}$$

where $K_1 = K_1^\top > 0$ (positive definite matrix), $I = I_0 + I_A = [I_1^\top, I_2^\top, I_3^\top]^\top$.

The partial derivative of H are

$$\frac{\partial H^\top}{\partial \tilde{\eta}_2} = K_1 \tilde{\eta}_2 \tag{35}$$

$$\frac{\partial H^\top}{\partial (I\tilde{v}_2)} = I\tilde{v}_2 \tag{36}$$

Then, the derivatives of the reference attitude (33) are

$$\begin{aligned} \dot{\tilde{\eta}}_2 &= \dot{\eta}_2 - \dot{\eta}_{2d} \\ &= J_2(\eta_2)v_2 - J_2(\eta_2)(v_2 - \tilde{v}_2) \\ &= J_2(\eta_2)\tilde{v}_2 \\ &= J_2(\eta_2)I^{-1}I\tilde{v}_2 \\ &= J_2(\eta_2)I^{-1}\frac{\partial H^\top}{\partial \tilde{v}_2} \end{aligned} \tag{37}$$

$$\dot{\tilde{v}}_2 = \dot{v}_2 - \dot{J}_2(\eta_2)\dot{\eta}_{2d} - J_2(\eta_2)\dot{\tilde{\eta}}_2 \tag{38}$$

The product of I and \dot{v}_2 is

$$\begin{aligned}
 I\dot{v}_2 &= I\dot{v}_2 - I\dot{J}_2(\eta_2)\dot{\eta}_{2d} - IJ_2(\eta_2)\ddot{\eta}_{2d} \\
 &= S(v_2)Iv_2 - Dv_2 + \tau_m - I\dot{J}_2(\eta_2)\dot{\eta}_{2d} - IJ_2(\eta_2)\ddot{\eta}_{2d} \\
 &= S(v_2)I(\tilde{v}_2 + J_2^{-1}(\eta_2)\dot{\eta}_{2d}) - Dv_2 + \tau_m - I\dot{J}_2(\eta_2)\dot{\eta}_{2d} - IJ_2(\eta_2)\ddot{\eta}_{2d} \\
 &= S(v_2)I\tilde{v}_2 + S(v_2)IJ_2^{-1}(\eta_2)\dot{\eta}_{2d} - Dv_2 + \tau_m - I\dot{J}_2(\eta_2)\dot{\eta}_{2d} - IJ_2(\eta_2)\ddot{\eta}_{2d} \\
 &\quad + I^{-1}J_2^\top(\eta_2)K_1\tilde{\eta}_2 - I^{-1}J_2^\top(\eta_2)K_1\tilde{\eta}_2 \\
 &= S(v_2)\frac{\partial H^\top}{\partial \tilde{v}_2} - I^{-1}J_2^\top(\eta_2)\frac{\partial H^\top}{\partial \tilde{\eta}_2} + \tau_m - \mathcal{M} + \kappa
 \end{aligned} \tag{39}$$

where

$$\mathcal{M} = Dv_2 \tag{40}$$

$$\kappa = S(v_2)IJ_2^{-1}(\eta_2)\dot{\eta}_{2d} - I\dot{J}_2(\eta_2)\dot{\eta}_{2d} - IJ_2(\eta_2)\ddot{\eta}_{2d} + I^{-1}J_2^\top(\eta_2)K_1\tilde{\eta}_2 \tag{41}$$

in which $J_2(\eta_2)$ can be obtained as follows

$$\dot{J}_2(\eta_2) = -S(v_2)J_2(\eta_2) \tag{42}$$

Then, the attitude error system is

$$\begin{bmatrix} \dot{\tilde{\eta}}_2 \\ I\dot{\tilde{v}}_2 \end{bmatrix} = \begin{bmatrix} 0_{3 \times 3} & J_2(\eta_2)I^{-1} \\ -I^{-1}J_2^\top(\eta_2) & S(v_2) \end{bmatrix} \begin{bmatrix} \frac{\partial H^\top}{\partial \tilde{\eta}_2} \\ \frac{\partial H^\top}{\partial(I\tilde{v}_2)} \end{bmatrix} + \begin{bmatrix} 0 \\ \tau_m - \mathcal{M} + \kappa \end{bmatrix} \tag{43}$$

The system states are $\tilde{\eta}_2$ and $I\tilde{v}_2$.

The η_2 state will follow η_{2d} if the system (43) converges to the zeros.

3.2. Controller and Estimator Design

Define unknown parameters $\vartheta = -[K_p, M_q, N_r]^\top$, which are the diagonal of D . The estimator error is

$$z_i = \hat{\vartheta}_i - \vartheta_i + \beta_i(v_{2i}) \tag{44}$$

where β_i is a continuous function.

For the convenience of controller design, we rewrite \mathcal{M} as

$$\mathcal{M} = Dv_2 = \begin{bmatrix} D_{11}v_{21} \\ D_{22}v_{22} \\ D_{33}v_{23} \end{bmatrix} = \begin{bmatrix} \vartheta_1\rho_1(v_{21}) \\ \vartheta_2\rho_2(v_{22}) \\ \vartheta_3\rho_3(v_{23}) \end{bmatrix} \tag{45}$$

where ρ_i is a continuous function.

The controller can be constructed as

$$\tau_m = \begin{bmatrix} (\hat{\vartheta}_1 + \beta_1(v_{21}))\rho_1(v_{21}) \\ (\hat{\vartheta}_2 + \beta_2(v_{22}))\rho_2(v_{22}) \\ (\hat{\vartheta}_3 + \beta_3(v_{23}))\rho_3(v_{23}) \end{bmatrix} - \kappa - K_2I\tilde{v}_2 \tag{46}$$

where K_2 is a positive-defined matrix valued function.

With the control input (46), the closed-loop system (43) can be written as

$$\begin{bmatrix} \dot{\tilde{\eta}}_2 \\ I\dot{\tilde{v}}_2 \end{bmatrix} = \begin{bmatrix} 0_{3 \times 3} & J_2(\eta_2)I^{-1} \\ -I^{-1}J_2^\top(\eta_2) & S(v_2) - K_2 \end{bmatrix} \begin{bmatrix} \frac{\partial H^\top}{\partial \tilde{\eta}_2} \\ \frac{\partial H^\top}{\partial(I\tilde{v}_2)} \end{bmatrix} - \begin{bmatrix} 0 \\ \Delta \end{bmatrix} \tag{47}$$

where

$$\Delta_i = z_i \rho_i(v_{2i}) \tag{48}$$

The estimator can be designed as

$$\dot{\hat{\vartheta}}_i = -\frac{\partial \beta_i}{\partial (v_{2i})} [\dot{v}_{2i} + \Delta_i] \tag{49}$$

We can see that Δ_i can be obtained from (47), which is

$$\begin{aligned} I\dot{v}_2 + \Delta &= I\dot{v}_2 + \begin{bmatrix} -I^{-1}J_2^\top \eta_2 & S(v_2) - K_2 \end{bmatrix} \begin{bmatrix} \frac{\partial H^\top}{\partial \tilde{\eta}_2} \\ \frac{\partial H^\top}{\partial I\tilde{v}_2} \end{bmatrix} - I\dot{\tilde{v}}_2 \\ &= \begin{bmatrix} -I^{-1}J_2^\top \eta_2 & S(v_2) - K_2 \end{bmatrix} \begin{bmatrix} K_1 \tilde{\eta}_2 \\ I\tilde{v}_2 \end{bmatrix} + \dot{J}_2(\eta_2)\eta_{2d} + J_2(\eta_2)\dot{\eta}_{2d} \end{aligned} \tag{50}$$

As a result, $[I_i\dot{v}_2 + \Delta_i]$ in (49) is a function of $v_2, \eta_2, \dot{\eta}_{2d}, \ddot{\eta}_{2d}$, and they are measurable or can be calculated from the given reference signal.

The continuous function β_i can be selected as

$$\beta_i(I_i v_2) = \gamma_i \int_0^{v_{2i}} \rho_i(\zeta) d\zeta = \frac{1}{2} \gamma_i v_{2i}^2 \tag{51}$$

where $\gamma_i > 0$, which implies that

$$\frac{\partial \beta_i}{\partial v_{2i}} = \gamma_i \rho_i(v_{2i}) \tag{52}$$

The control scheme is illustrated in Figure 2.

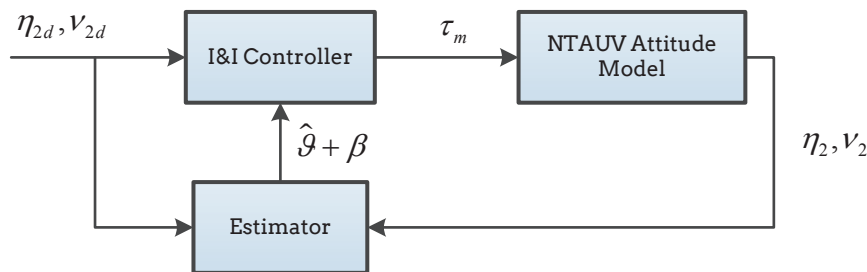


Figure 2. I&I control scheme.

3.3. Stability Analysis

The derivative of (44) is

$$\begin{aligned} \dot{z}_i &= \dot{\hat{\vartheta}}_i - \dot{\vartheta}_i + \dot{\beta}_i(v_{2i}) \\ &= -\frac{\partial \beta_i}{\partial (v_{2i})} [\dot{v}_{2i} + z_i \rho_i(v_{2i})] + \frac{\partial \beta_i}{\partial (v_{2i})} (v_{2i}) \\ &= -\gamma_i \rho_i(v_{2i}) \rho_i(v_{2i}) z_i \end{aligned} \tag{53}$$

where ϑ_i is assumed to be a constant.

The Lyapunov function is $W(z) = \sum_{i=1}^3 \frac{1}{\gamma_i} |z_i|^2$, then

$$\begin{aligned} \dot{W}(z) &= \sum_{i=1}^3 \frac{2}{\gamma_i} z_i \dot{z}_i \\ &= \sum_{i=1}^3 \frac{2}{\gamma_i} z_i (-\gamma_i \rho_i(v_{2i}) \rho_i(v_{2i}) z_i) \\ &= -2 \sum_{i=1}^3 z_i \rho_i(v_{2i}) \rho_i(v_{2i}) z_i \\ &= -2 \Delta^\top \Delta \\ &= -2 |\Delta|^2 \leq 0 \end{aligned} \tag{54}$$

which means that $\hat{\vartheta} \rightarrow \vartheta$ as $t \rightarrow \infty$.

We want the whole system to be stable, which means $(\tilde{\eta}_2, \tilde{v}_2, z)^\top$ has the equilibrium point $(0, 0, 0)^\top$ that is stable.

Consider the Lyapunov function $V = H(\tilde{\eta}_2, \tilde{v}_2) + W(z)$. The derivative of V is

$$\begin{aligned} \dot{V} &= \frac{\partial H}{\partial \tilde{\eta}_2} \dot{\tilde{\eta}}_2 + \frac{\partial H}{\partial (I\tilde{v}_2)} (I\dot{\tilde{v}}_2) + \dot{W}(z) \\ &= \frac{\partial H}{\partial \tilde{\eta}_2} J_2(\eta_2) I^{-1} \frac{\partial H^\top}{\partial \tilde{v}_2} + \frac{\partial H}{\partial (I\tilde{v}_2)} (-I^{-1} J_2^\top(\eta_2) \frac{\partial H^\top}{\partial \tilde{\eta}_2} + (S(v_2) - K_2) \frac{\partial H^\top}{\partial \tilde{v}_2} - \Delta) - 2 \Delta^\top \Delta \\ &= \frac{\partial H}{\partial (I\tilde{v}_2)} (-K_2 \frac{\partial H^\top}{\partial \tilde{v}_2} - \Delta) - 2 \Delta^\top \Delta \\ &= -\frac{\partial H}{\partial (I\tilde{v}_2)} K_2 \frac{\partial H^\top}{\partial \tilde{v}_2} - \frac{\partial H}{\partial (I\tilde{v}_2)} \Delta - 2 \Delta^\top \Delta \\ &= -\frac{\partial H}{\partial (I\tilde{v}_2)} (K_2 - \frac{1}{2\sqrt{2}} I_{3 \times 3}) \frac{\partial H^\top}{\partial \tilde{v}_2} - \frac{\partial H}{\partial (I\tilde{v}_2)} (\frac{1}{2\sqrt{2}} I_{3 \times 3}) \frac{\partial H^\top}{\partial \tilde{v}_2} - \frac{\partial H}{\partial (I\tilde{v}_2)} \Delta - 2 \Delta^\top \Delta \end{aligned}$$

select K_2 such that $K_2 - \frac{1}{2\sqrt{2}} I_{3 \times 3} > 0$; then, $\dot{V} \leq 0$.

4. Experiment Results

4.1. Testbed

A 3 DOF testbed is designed for verifying the performance of the presented controller. The testbed includes three parts: the unmovable base, 3-DOF ball joint, and NTAUV. The ball joint enables a maximum $\pm 40^\circ$ roll and pitch angle and 360° yaw angle. The 3 DOF ball joint of the testbed is illustrated in Figure 3.

The mechanical parameters of the NTAUV are listed in Table 1.

We designed our own control system. A desktop PC running ground station software was used as the host computer. This computer sends commands and receives attitude data via a serial port. An STM32 Nucleo F401RE board, with 512 KB memory and 84 MHz CPU frequency is used as the controller board. The computation power guarantees the capability to apply an advanced control algorithm, dealing with complex matrix calculation running at 100 Hz.

The attitude sensor module reads raw three-axis accelerometers, gyroscopes, and magnetometers data from MPU9250, runs a Kalman filter algorithm, and sends the attitude and angular speed to the controller board. The rotor is a brushless DC motor; a propeller is mounted on the top of the motor, and it can provide maximum thrust of 15 N. The servo provides a maximum torque of 0.15 N·m, and the maximum speed of rotation is 6.9 rad/s.

Table 1. Mechanical parameters of NTAUV.

Parameters	Value	Unit (SI)
l_1	0.13	m
l_2	0.075	m
l_3	0.15	m
m	1	kg
B	3	N
I_{xx}	0.0061	kg/m ²
I_{yy}	0.006	kg/m ²
I_{zz}	0.0118	kg/m ²

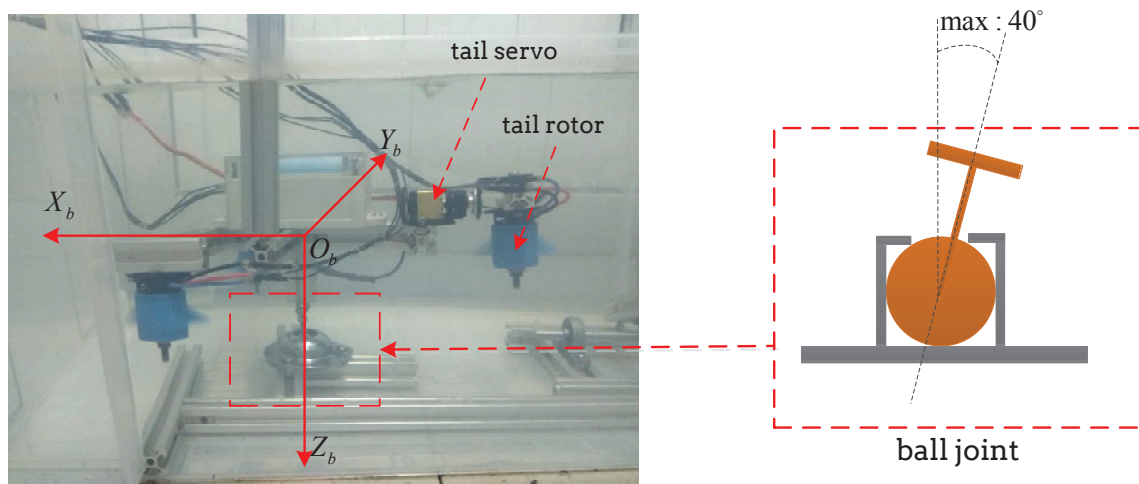


Figure 3. Testbed.

4.2. Experiment Results and Discussion

Attitude control is essential for under actuated rigid body vehicles, such as airplanes, surface vessels, helicopters, and multi-rotor aerial vehicles. Attitude control is often designed as the inner loop of path or trajectory control, named as hierarchical control. η_{2d} is the output of the higher layer controller. As a fundamental function of attitude control, $\eta_{2d} = [0, 0, 0]^T$ is an essential state that needs to be stabilized under the influence of disturbance, such as hydrodynamic moments generated by constant fluent or turbulence, and collision.

4.2.1. I&I Control Experiment

The parameters of the I&I controller are selected as follows: $K_1 = \text{diag}\{0.02, 0.1, 0.03\}$, $K_2 = \text{diag}\{5, 5, 5\}$, $\gamma = [0.4, 0.4, 0.4]^T$.

To validate the anti-disturbance performance of I&I controller, disturbances are applied to each axis. Each axis is disturbed by a collision. The I&I controller regulates the state to $\eta_2 = [0, 0, 0]^T$. The roll, pitch, and yaw control results of I&I control are shown in Figure 4.

The experiment results show that: (1) the attitude error generated by the collision is near 10°; (2) the attitude converges to η_{2d} in less than 0.8 s; (3) the roll and pitch control have shorter adjust time than the yaw control, which is because the yaw axis has a higher moment of inertia and a lower control moment, resulting from the mechanical design of the rotor arrangement; and (4) when no disturbance is applied, the control accuracy of roll and pitch is better than yaw; this is mainly for the unmodeled dynamics of the tail servo.

The control torque is shown in Figure 5. The roll and pitch control torques are generated by the change in the speed of the rotors, which is quick, whereas the yaw control torque is generated by the servo sway, which is slow and has a slight chattering.

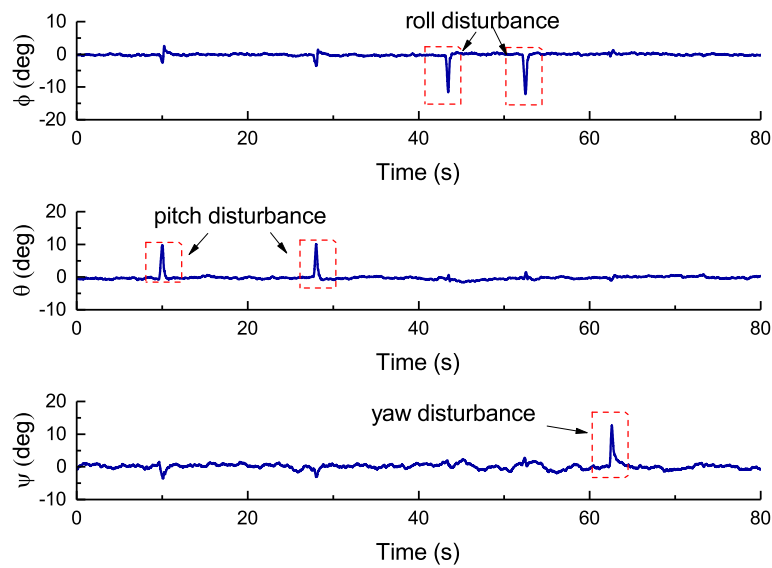


Figure 4. Attitude of NTAUV under I&I control with disturbance on each axis.

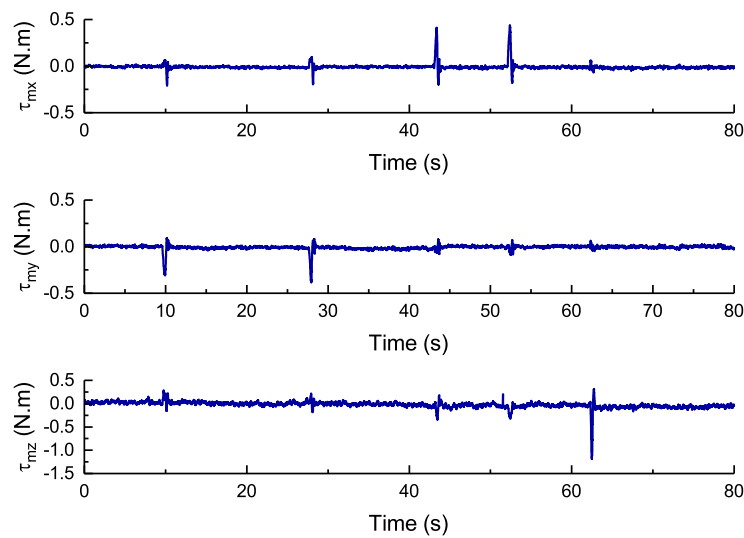


Figure 5. I&I control torque.

4.2.2. PI Control Experiment

We compare experiment results generated by the I&I controller with the ones generated by the typical cascaded proportional integral (PI) controller. The parameters of PI controller are selected carefully to get good performance. The parameters of PI approach are as follows: angular velocity loop controller $k_p^v = 0.2, k_i^v = 1$, angular position loop controller $k_p^p = 0.08, k_i^p = 0.001$. The experiment results of PI control are shown in Figures 6 and 7. It shows that it takes more than 1.3 s to converge to desired attitude, and the yaw control takes even more than 3 s.

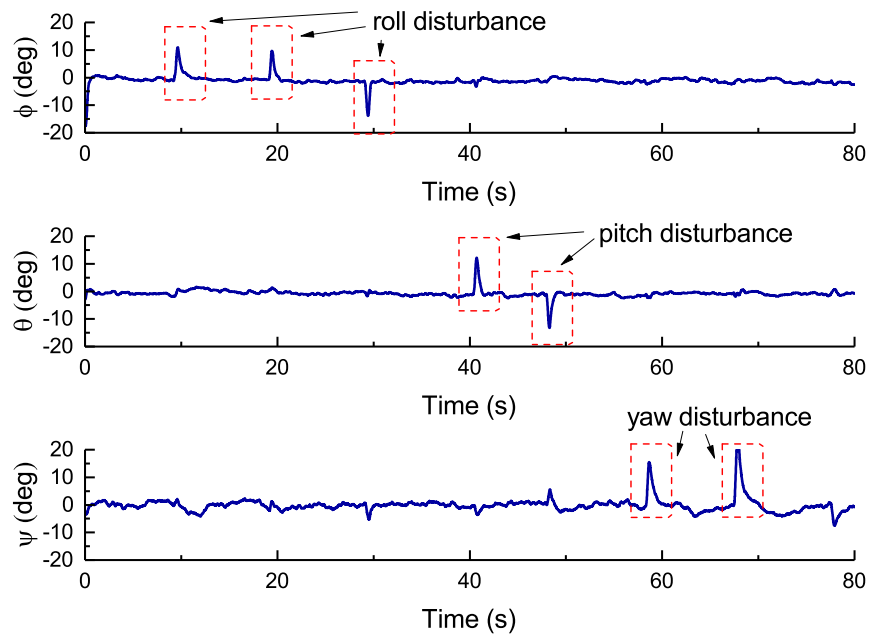


Figure 6. Attitude of NTAUV under PI control with disturbance on each axis.

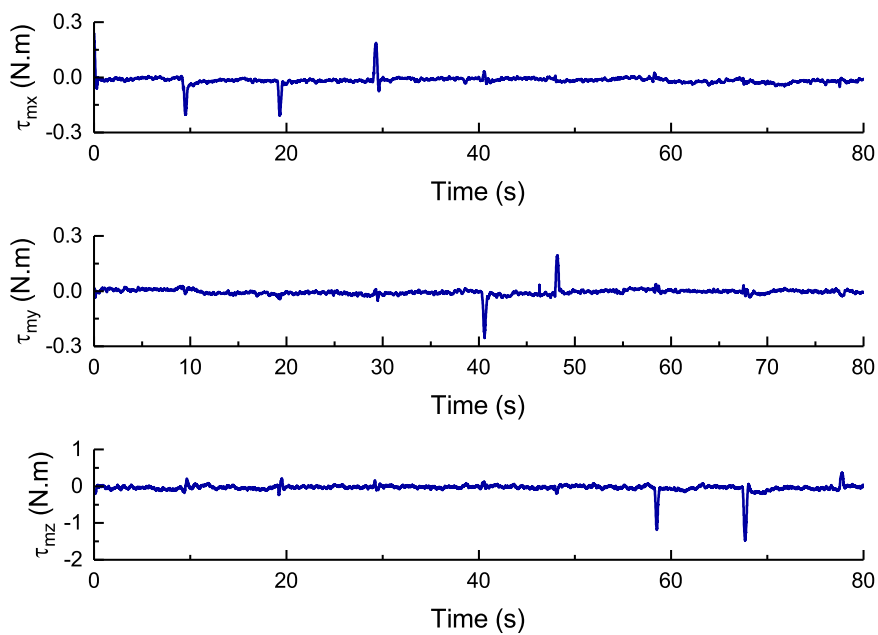


Figure 7. PI control torque.

4.2.3. Comparison Between I&I and PI Control

The comparisons of the roll, pitch and yaw control performance between I&I and PI control are shown separately in Figures 8–10. The I&I control performs higher accuracy than PI control under disturbance.

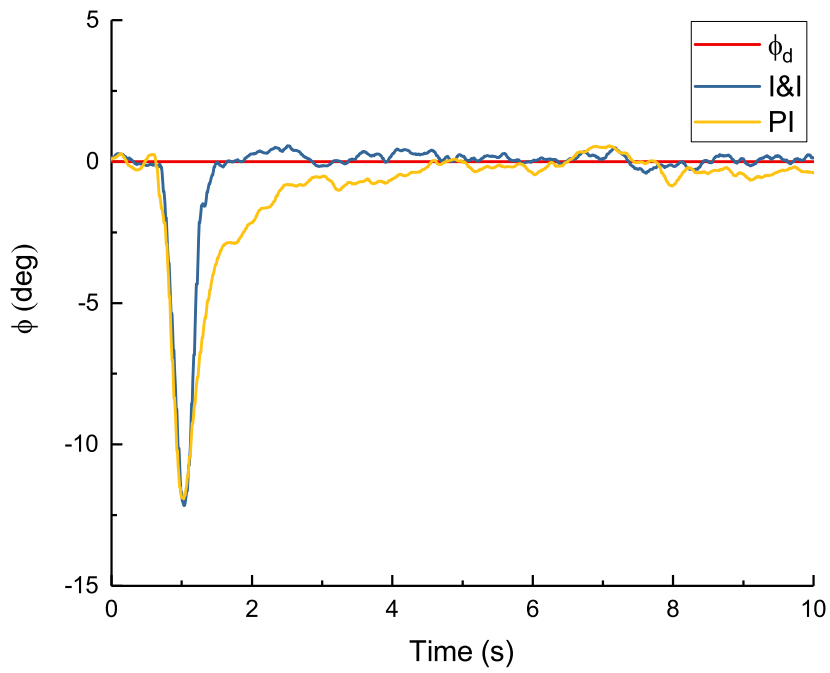


Figure 8. Roll Control Comparison between I&I and PI Control.

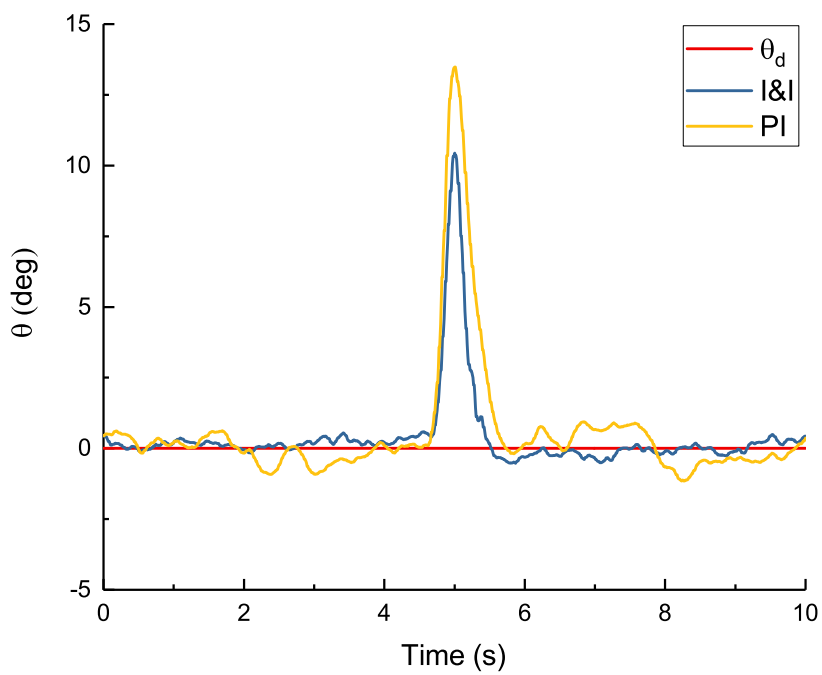


Figure 9. Pitch Control Comparison between I&I and PI Control.

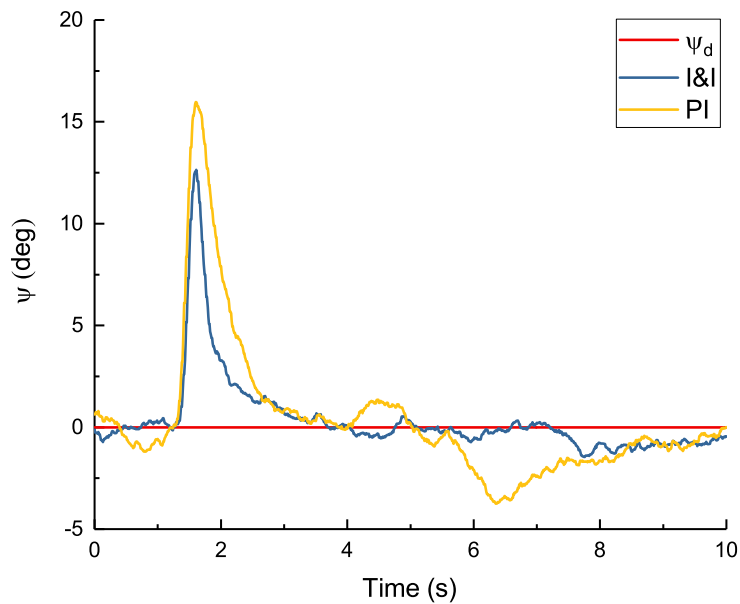


Figure 10. Yaw Control Comparison between I&I and PI Control.

The hydrodynamic force and moment are complex as the underwater vehicle works at a low Reynolds number (Re) condition, especially when hovering and for low-speed horizontal moving. The actual hydrodynamic force is very complex, because there is no stable flow field around. The disturbance rejection performance of I&I control is validated.

5. Conclusions

In this paper, a negative-buoyancy tri-tilt-rotor autonomous underwater vehicle was presented and an attitude controller was designed for attitude stabilization. The full mathematical model of the NTAUV was established, and it was decoupled to attitude and altitude subsystems. Then, the attitude subsystem was investigated, and an adaptive attitude controller was designed based on the I&I theory. A parameter estimator was applied to estimate the unknown parameters. The global stability of the controller was proved. Finally, the performance of the proposed controller was validated through a real-time attitude stabilization experiment. The experimental results indicated a satisfactory performance compared with a well designed PID controller.

Author Contributions: T.W. put forward the original concept, proposed the control approach, and wrote the article. C.W., T.G., J.W. and T.G. gave their valuable suggestions on research design. Further, T.W., C.W. and J.W., analyzed and discussed the experimental results.

Funding: This work is supported by the National Natural Science Foundation of the National Research and Development of major scientific instruments (41427806), the National Natural Science Foundation of China (Grant No. 51779139), the National Key Research and Development Program of China (Grant No. 2016YFC0300700), ROV System For Exploration and Sampling (DY125-21-Js-06) funded by the State Oceanic Administration People's Republic of China and National High Technology Research and Development Program of China (863 Program, Grant No. 2012AA092103).

Acknowledgments: The authors would also like to express their appreciation to Chunwen Zhang and Han Liu for their considerable help on the experiment.

Conflicts of Interest: The authors declare no conflict of interest.

References

1. Fossen, T. *Guidance and Control of Ocean Vehicles*; John Willey & Sons: Hoboken, NJ, USA, 1994.

2. Li, X.; Zhao, M.; Ge, T. A Nonlinear Observer for Remotely Operated Vehicles with Cable Effect in Ocean Currents. *Appl. Sci.* **2018**, *8*, 867. [[CrossRef](#)]
3. Wu, N.; Wu, C.; Ge, T.; Yang, D.; Yang, R. Pitch Channel Control of a REMUS AUV with Input Saturation and Coupling Disturbances. *Appl. Sci.* **2018**, *8*, 253. [[CrossRef](#)]
4. Salgado-Jimenez, T.; Gonzalez-Lopez, J.L.; Pedraza-Ortega, J.C.; García-Valdovinos, L.G.; Martínez-Soto, L.F.; Resendiz-Gonzalez, P.A. Design of ROVs for the Mexican power and oil industries. In Proceedings of the 2010 1st International Conference on Applied Robotics for the Power Industry, Montreal, QC, Canada, 5–7 October 2010; pp. 1–8.
5. Soylu, S.; Proctor, A.A.; Podhorodeski, R.P.; Bradley, C.; Buckham, B.J. Precise trajectory control for an inspection class ROV. *Ocean Eng.* **2016**, *111*, 508–523. [[CrossRef](#)]
6. Wynn, R.B.; Huvenne, V.A.I.; Le Bas, T.P.; Murton, B.J.; Connelly, D.P.; Bett, B.J.; Ruhl, H.A.; Morris, K.J.; Peakall, J.; Parsons, D.R.; et al. Autonomous Underwater Vehicles (AUVs): Their past, present and future contributions to the advancement of marine geoscience. *Mar. Geol.* **2014**, *352*, 451–468. [[CrossRef](#)]
7. Palomeras, N.; Vallicrosa, G.; Mallios, A.; Bosch, J.; Vidal, E.; Hurtos, N.; Carreras, M.; Ridao, P. AUV homing and docking for remote operations. *Ocean Eng.* **2018**, *154*, 106–120. [[CrossRef](#)]
8. Liu, K.; Huang, Y.; Zhao, Y.; Cui, S.; Wang, X.; Wang, G. Research on error correction methods for the integrated navigation system of deep-sea human occupied vehicles. In Proceedings of the OCEANS 2015—MTS/IEEE Washington, Washington, DC, USA, 19–22 October 2015; pp. 1–5.
9. Hosseini, M.; Seyedtabaai, S. Robust ROV path following considering disturbance and measurement error using data fusion. *Appl. Ocean Res.* **2016**, *54*, 67–72. [[CrossRef](#)]
10. Cui, R.; Zhang, X.; Cui, D. Adaptive sliding-mode attitude control for autonomous underwater vehicles with input nonlinearities. *Ocean Eng.* **2016**, *123*, 45–54. [[CrossRef](#)]
11. Cui, R.; Li, Y.; Yan, W. Mutual Information-Based Multi-AUV Path Planning for Scalar Field Sampling Using Multidimensional RRT. *IEEE Trans. Syst. Man Cybern. Syst.* **2016**, *46*, 993–1004. [[CrossRef](#)]
12. Cui, R.; Yang, C.; Li, Y.; Sharma, S. Adaptive Neural Network Control of AUVs With Control Input Nonlinearities Using Reinforcement Learning. *IEEE Trans. Syst. Man Cybern. Syst.* **2017**, *47*, 1019–1029. [[CrossRef](#)]
13. Nouri, N.M.; Valadi, M. Robust input design for nonlinear dynamic modeling of AUV. *ISA Trans.* **2017**, *70*, 288–297. [[CrossRef](#)] [[PubMed](#)]
14. Paull, L.; Saeedi, S.; Seto, M.; Li, H. AUV Navigation and Localization: A Review. *IEEE J. Ocean. Eng.* **2014**, *39*, 131–149. [[CrossRef](#)]
15. Hussain, N.A.A.; Arshad, M.R.; Mohd-Mokhtar, R. Underwater glider modelling and analysis for net buoyancy, depth and pitch angle control. *Ocean Eng.* **2011**, *38*, 1782–1791. [[CrossRef](#)]
16. Brown, C.L. Deep sea mining and robotics: Assessing legal, societal and ethical implications. In Proceedings of the 2017 IEEE Workshop on Advanced Robotics and its Social Impacts (ARSO), Austin, TX, USA, 8–10 March 2017; pp. 1–2.
17. Javaid, M.Y.; Ovinis, M.; Hashim, F.B.M.; Maimun, A.; Ahmed, Y.M.; Ullah, B. Effect of wing form on the hydrodynamic characteristics and dynamic stability of an underwater glider. *Int. J. Naval Archit. Ocean Eng.* **2017**, *9*, 382–389. [[CrossRef](#)]
18. Li, Y.; Pan, D.; Zhao, Q.; Ma, Z.; Wang, X. Hydrodynamic performance of an autonomous underwater glider with a pair of bioinspired hydro wings—A numerical investigation. *Ocean Eng.* **2018**, *163*, 51–57. [[CrossRef](#)]
19. Tchilian, R.D.S.; Rafikova, E.; Gafurov, S.A.; Rafikov, M. Optimal Control of an Underwater Glider Vehicle. *Procedia Eng.* **2017**, *176*, 732–740. [[CrossRef](#)]
20. Bessa, W.M.; Dutra, M.S.; Kreuzer, E. An adaptive fuzzy sliding mode controller for remotely operated underwater vehicles. *Robot. Auton. Syst.* **2010**, *58*, 16–26. [[CrossRef](#)]
21. Campos, E.; Monroy, J.; Abundis, H.; Chemori, A.; Creuze, V.; Torres, J. A nonlinear controller based on saturation functions with variable parameters to stabilize an AUV. *Int. J. Naval Archit. Ocean Eng.* **2018**. [[CrossRef](#)]
22. Yan, H.; Ge, T.; Li, J.W.; Wang, Q. Prediction of mode and static stability of negative buoyancy vehicle. In Proceedings of the 2011 Chinese Control and Decision Conference (CCDC), Mianyang, China, 23–25 May 2011; pp. 1903–1909.
23. Ji, S.W.; Bui, V.P.; Balachandran, B.; Kim, Y.B. Robust control allocation design for marine vessel. *Ocean Eng.* **2013**, *63*, 105–111. [[CrossRef](#)]

24. Xiang, X.; Lapierre, L.; Jouvencel, B. Smooth transition of AUV motion control: From fully-actuated to under-actuated configuration. *Robot. Auton. Syst.* **2015**, *67*, 14–22. [[CrossRef](#)]
25. Xiang, X.; Yu, C.; Zhang, Q. Robust fuzzy 3D path following for autonomous underwater vehicle subject to uncertainties. *Comput. Oper. Res.* **2017**, *84*, 165–177. [[CrossRef](#)]
26. Salazar-Cruz, S.; Kendoul, F.; Lozano, R.; Fantoni, I. Real-time stabilization of a small three-rotor aircraft. *IEEE Trans. Aerosp. Electron. Syst.* **2008**, *44*, 783–794. [[CrossRef](#)]
27. Papachristos, C.; Tzes, A. Modeling and control simulation of an unmanned Tilt Tri-Rotor Aerial vehicle. In Proceedings of the 2012 IEEE International Conference on Industrial Technology, Athens, Greece, 19–21 March 2012; pp. 840–845.
28. Ta, D.A.; Fantoni, I.; Lozano, R. Modeling and control of a tilt tri-rotor airplane. In Proceedings of the 2012 American Control Conference (ACC), Montreal, QC, Canada, 27–29 June 2012; pp. 131–136.
29. Astolfi, A.; Ortega, R. Immersion and invariance (I2): A new tool in nonlinear control design. In Proceedings of the 2001 European Control Conference (ECC), Porto, Portugal, 4–7 September 2001; pp. 2854–2859.
30. Astolfi, A.; Ortega, R. Immersion and invariance: A new tool for stabilization and adaptive control of nonlinear systems. *IEEE Trans. Autom. Control* **2003**, *48*, 590–606. [[CrossRef](#)]
31. Astolfi, A.; Karagiannis, D.; Ortega, R. *Nonlinear and Adaptive Control with Applications*; Springer: Berlin/Heidelberg, Germany, 2008.



© 2018 by the authors. Licensee MDPI, Basel, Switzerland. This article is an open access article distributed under the terms and conditions of the Creative Commons Attribution (CC BY) license (<http://creativecommons.org/licenses/by/4.0/>).